Electronic Supplementary Material (ESI) for Physical Chemistry Chemical Physics.
This journal is © the Owner Societies 2016

Simulations of Molecular Self-Assembled Monolayers on Surfaces: Packing Structures, Formation Processes and Functions Tuned by Intermolecular and Interfacial Interactions

Jin Wen,[a] Wei Li,[a] Shuang Chen[b] and Jing Ma[a*]

[a.] Institute of Theoretical and Computational Chemistry, Key Laboratory of Mesoscopic Chemistry of MOE, School of Chemistry and Chemical Engineering, Nanjing University, Nanjing 210093, P. R. China

[b.] Kuang Yaming Honors School, Nanjing University, Nanjing, Jiangsu 210023, P. R. China

Supporting Information

S1. Computational Details in the SAM modeling

Table S1. Comparisons of canonical MP2, GEBF-MP2, and GEBF-MP2/HF relative energies (in a.u.) and relative energies (in kcal·mol^{-1}) with respective to the HH dimer of different arrangements (HH, HT, and TT) for 5T.

Table S2. Comparisons of canonical MP2, GEBF-MP2, and GEBF-MP2/HF relative energies ΔE (in kcal·mol^{-1}) with respective to the HH dimer and binding energies E_b (in kcal·mol^{-1}) of different arrangements (HH, HT, and TT) for 5T.

Table S3. Quadrupole moments Q (in the unit of a.u.), dipole-dipole interaction ($E_{\mu\mu}$), ratio between electrostatics and van der Waals interactions in the force filed ($E_{ele.}/E_{vdw}$), and order index (S_{ij}) in 5Ts monomer, dimers, and monolayers. The dipole interaction is defined in Figure S1.

Table S4 Quadrupole moments (in the unit of a.u.) of 5T monomers and dimers in different arrangements at M06-2X/6-31G* level.

Figure S1. Definition of dipole-dipole interaction, $E_{\mu\mu}$.

Figure S2. Fragments in the GEBF method.

Figure S3. Statistical analysis in 5Ts monolayers on the HOPG surface, (a) torsion angle distribution, (b) radial distribution function, (c) inclination angle distribution, and (d) orientation angle distribution.

Figure S4. Distribution of HH, HT, and TT arrangements of 5T monolayers on the HOPG surface.

Figure S5. Initial configurations of self-assembled (a) CA monolayer on Ag(111) surface and (b) RA monolayer on Au(111) surface in our AIMD simulations. The applied electric fields for each slab model are highlighted in insets.

Figure S6. Illustration of two cutoffs for estimation of z component of polarization by using the charge density integral method.

S1. Computational Details in the SAM modeling

S1.1 Computational details in the QM and MD simulations of 5Ts/HOPG system

We performed GEBF-MP2 and GEBF-MP2/HF[1] single point calculations at the GEBF-M06-2X optimized geometry for 5Ts. The total system was divided in to five fragments by cutting the valence bonds in thiophene unit, as displayed in Figure S1. In the GEBF-M06-2X and GEBF-MP2 calculations, a distance threshold was set as 3.5Å and the 6-31G(d) basis set was employed. All the GEBF calculations were carried out with low scaling quantum chemistry (LSQC) program[2,3] and the calculations of subsystems were performed with Gaussian 09 package.[4]

In the MD simulations, PCFF was adopted in the molecular dynamics simulations to study the morphology of 5T monolayer on HOPG surface. The surface was fixed, without considering its reconstruction. We put 34 chains of 5T-br and 33 chains of 5T-cho on four layers of HOPG surfaces in an 85.22×98.40×40.20 $Å^3$ periodical slab box, respectively. MD simulations were performed in the canonical (NVT) ensemble in Material Studios program.[5] In order to reproduce the experimental condition, we used annealing process, by using an Andersen thermostat[2] at 350 K. The equations of motion were integrated by the velocity Verlet method[3] with the time step of 1 fs. The 1 ns MD trajectories are collected after the equilibrium stage at every 100 fs at 298 K with the statistical analysis results shown in Fig. S3-S4.

S1.2 Estimation of Polarization of CA and RA Monolayers

The AIMD simulations are performed in the framework of density functional theory (DFT) with generalized gradient approximation (GGA) for the exchange-correlation functional in the Perdew-Burke-Ernzenhof (PBE) form, as implemented in the DMol[3] module of Materials Studio 7.0. The electric field as large as 10^{10} V/m can be applied in the AIMD simulations to investigate the influence of external electric field on the self-assembled CA monolayer on Ag(111) surface or RA monolayer on Au(111) surface. As shown in Fig. S5, for CA monolayer on Ag(111), the in-plane electric field is applied along the *x* direction, while for RA monolayer on Au(111), the in-plane electric field is along the *y* direction. Also, the electric fields perpendicular to the metal surfaces (both *z* and −*z*) are applied to the two model systems. The AIMD simulations are carried out using periodic boundary conditions. The slab models for CA monolayer on Ag(111) and RA monolayer on Au(111) are taken from Kunkel et al.'s work.[8,9] The further DMol[3]-optimized CA and RA

monolayers on metal surfaces are taken as the initial configurations for our AIMD simulations. Due to high computing cost of AIMD simulations, all atoms of metal substrates are fixed. The vacuum layer is about 20 Å in each system. The Brillouin zones for the slab models are only sampled at the Γ point for the AIMD simulations. The Tkatchenko-Scheffler (TS) dispersion correction[10] is adopted to account for weak van der Waals (vdW) interactions. The dipole slab correction is added along the direction perpendicular to the substrate. The double numerical basis set plus polarization (DNP) is selected along with the effective-core potential (ECP) for treating core electrons. The global real space cutoff is set as 4.5 Å. The self-consistent field (SCF) convergence is set to 10^{-6} a.u., and the thermal smearing with 0.005 Ha is applied to the orbital occupation to speed up convergence. Each AIMD simulation is performed in the canonical (*NVT*) ensemble with the temperature controlled at 298.15 K by using the Nosé-Hoover chain thermostat (Q ratio = 2.0 and chain length = 3). The time step is set as 1 fs.

Based on the AIMD trajectories, we select various, specific structural configurations of CA monolayer or RA monolayer. Subsequently, the Berry phase method, as implemented in VASP 5.3.5, is used to compute the polarization of selected CA monolayer or RA monolayer along the *x* and *y* directions without the metal substrate. The total spontaneous polarization is decomposed into ionic and electronic contributions, $P_{\mathrm{Berry}} = P_{\mathrm{ion}} + P_{\mathrm{e}}$. For the polarization along the *z* direction, the Berry phase method is not applicable due to the presence of a vacuum layer. Hence, the charge density integral method is employed to estimate the *z* component of polarization and to further correct the *x* and *y* components of polarization from the Berry phase method based on the two-time charge density calculations of the supercells with and without the metal substrate, respectively. The Berry phase method, combined with charge density integral, gives us the three components of the polarization vector.

To compute the charge density integral of organic monolayer, the integral interval depends on two cutoffs in Fig. S6: one, organic monolayer/metal substrate interface, which is set to the height of metal atoms in the first layer plus vdW radius of metal atom, and the other, vacuum/organic monolayer interface, which is set to the *z* coordinate of the highest atom within the organic monolayer plus vdW radius of carbon atom. For estimation of the *z* component of the polarization, the effect of charge transfer between metal substrate and organic monolayer

has been included. Based on the charge density integral method, the polarization difference between one with metal substrate and one without from the two-time charge density integral calculations, $\Delta P = P_{\text{with}} - P_{\text{without}}$, can be used here to approximately correct the Berry phase results for *x* and *y* components as $P_{x(y)} = P_{\text{Berry}} + \Delta P$ from the contribution of charge-transfer interaction. The final corrected polarization changes for different configurations with respect to the initial configurations of CA and RA monolayers are presented in Ref 41 of the main text. For both the polarization and charge density calculations in VASP, the convergence condition in SCF iteration is set to be less than 10^{-6} eV. The PBE-D3 method is used to account for vdW interactions. The electron-ion interaction is described by the projector augmented wave (PAW) potentials with an energy cutoff of 600 eV. The Brillouin zones are sampled using a 8×8×1 k-point mesh within the Monkhorst-Pack scheme.

S1.3 Theoretical Prediction of 3-HPLN Linear-Like and Honeycomb-Like Bilayer Structures on Cu(111) Surface

Linear-like bilayer **(Fig. 8d in the main text).** Based on the experimental scanning tunneling microscopy (STM) image of linear-chain network, (main text Ref 40) 3-HPLN molecules aligned in rows in the bottom layer through zipper-like hydrogen bonds, are deposited on 3-layer Cu(111) surface. In the top layer, the π–π stacked 3-HPLN dimer taken from the crystal structure stands upright on the bottom layer to form linear chains. In addition, this dimer occupies the zipper-liker hydrogen bonding channel of bottom layer and at the same time the O= and HO-containing ends of the top dimer points towards the bottom layer to form hydrogen bonds with 3-HPLN molecules in the bottom layer. In order to verify our built linear-chain model, the VASP optimization is performed. A more-than-20-Å vacuum layer is first added. The slab model is optimized by using the periodic DFT calculations by using the PBE form within the framework of GGA. The Grimme's correction (D2) is also adopted to account for vdW interactions. The electron-ion interaction is described by the PAW potentials with an energy cutoff of 500 eV. The Brillouin zones are sampled using a 3×3×1 k-point mesh in the Monkhorst-Pack scheme. The total energy change is required to be less than 10^{-5} eV, and the magnitude of the largest force acting on the atoms should be less than 0.05 eV/Å.

Honeycomb-like bilayer **(Fig. 8e in the main text).** In our previous work, (main text Ref 40) we have detailed analyzed the honeycomb-like bilayer structures. The 3-HPLN trimer is taken as the building unit to form the bottom layer with six-axis symmetry. This bottom layer is deposited on 1-layer Cu(111) surface (in consideration of computational expense). The π−π stacking 3-HPLN dimer is taken as the building unit to generate the pinwheel-like junctions consisting of three dimers and linear segments consisting of two dimers, which connects two junctions within the honeycomb-like network. Considering the symmetry of this Kagome-lattice top layer, all the 3-HPLN molecules in the top layer with their O= and HO-containing ends pointing towards the bottom layer stand up right on the bottom layer. A rhombus slab model with 20-Å vacuum layer is built, and its optimization is performed in the CP2K software. The PBE functional with the Gaussian plane-wave (GPW) method is employed to optimize the honeycomb-like bilayer. To better describe the long-range electron correlations that are responsible for the vdW interactions, the Grimme's correction (D2) is adopted. The core electrons are described by the Goedecker-Teter-Hutter (GTH) norm-conserving pseudopotential, and the wave functions of valence electrons are expressed by the combination of the polarized double-ξ quality Gaussian basis and a plane wave basis set. The auxiliary plane-wave basis set is defined by an energy cutoff of 330 Ry, accompanied by a relative cutoff of 33 Ry for Gaussian basis set collocation. The self-consistent field (SCF) convergence is set to 10^{-6} a.u.

S1.4 Computational details for entropy change of SAM formation

The Helmholtz free energy of the canonical (N, V, T) system has this form

$$F = U - TS \tag{S1}$$

We took the physical vapor deposition (PVD) growth of pentacene (Pn) as an example to illustrate calculations of the entropy and Helmholtz free energy of this process. We first performed MD simulations (NVT ensemble, room temperature) of dynamic growth of Pn monolayers on the amorphous SiO_2 surface to record corresponding trajectories for further entropy and free energy estimation. A quasi-static way by adding on Pn molecule at a time (τ_{add} = 400 ps) was employed by us to investigate the growth of Pn self-assembly monolayer (SAM). During this SAM formation process, a 400-ps MD trajectory for deposition of each Pn molecule on the SiO_2 surface was recorded each time. Based on the last 300-ps trajectories (equilibrium

stage), we first statistically analyzed the radial (r) and orientational (ω, φ) relationship between two Pn molecules (taken as a Pn pair) at the same time, and run this analysis for all the possible Pn pairs in the Pn SAM with a certain number of Pn molecules. After obtaining the $N_{\text{pair}}(r, \omega, \varphi)$ by the statistical analysis above, the pair distribution function $g(r, \omega, \varphi)$ was estimated according to Eq. (6) in the main text. Finally, the packing entropy, S_{pack}, for Pn SAM with a certain number of Pn molecules was calculated according to Eq. (7) in the main text by using the value of $g(r, \omega, \varphi)$, and changing the integral of Eq. (7) into the sum of $g(r, \omega, \varphi)\ln g(r, \omega, \varphi)$ for each value of $g(r, \omega, \varphi)$. Furthermore, S_{iso} for a single Pn molecule was estimated from the QM frequency calculation of an optimized Pn molecule. The contribution of entropy ($S = NS_{\text{iso}} + S_{\text{pack}}$) to Helmholtz free energy was approximated obtained according to Eq. (S1), by adding the estimated value of TS term to U term. The U term was the average total energy of investigated system (Pn molecules on SiO_2 surface) at the equilibrium stage learned from MD simulations.

Table S1. Comparisons of canonical MP2, GEBF-MP2, and GEBF-MP2/HF relative energies (in a.u.) and relative energies (in kcal·mol^{-1}) with respective to the HH dimer of different arrangements (HH, HT, and TT) for 5T.

	Canonical MP2[a]	GEBF-MP2[a]	GEBF-MP2/HF[a]
5T dimer			
HH	-6293.44566 (0.00)	-6293.44653 (0.00)	-6293.44393 (0.00)
HT	-6293.44266 (1.88)	-6293.44173 (3.01)	-6293.44211 (1.14)
TT	-6293.44008 (3.50)	-6293.44029 (3.92)	-6293.43960 (2.72)
5Ts pentamer			
5T-br		-41425.70648	-41425.71016
5T-cho		-16861.67221	-16861.67384

[a] The relative energies relative to the HH dimer included in parentheses.

Table S2. Comparisons of canonical MP2, GEBF-MP2, and GEBF-MP2/HF relative energies Δ*E* (in kcal·mol^{-1}) with respective to the HH dimer and binding energies E_b (in kcal·mol^{-1}) of different arrangements (HH, HT, and TT) for 5T.

	Canonical MP2		GEBF-MP2	GEBF-MP2/HF	
dimer	Δ*E*	E_b	Δ*E*	Δ*E*	
HH	0.00	-4.28	0.00	0.00	
HT	1.88	-2.39	3.01	1.14	
TT	3.50	-0.77	3.92	2.72	
NPE[a]	--		1.13	0.78	
pentamer				E_b	E_b
5T-br				-4.37	-5.01
5T-cho				-6.97	-7.51

[a]Nonparallelity error, relative to the canonical MP2 results, in kcal·mol^{-1}.

Table S3. Quadrupole moments Q (in the unit of a.u.), dipole-dipole interaction ($E_{\mu\mu}$), ratio between electrostatics and van der Waals interactions in the force filed ($E_{ele.}/E_{vdw}$), and order index (S_{ij}) in 5Ts monomer, dimers, and monolayers. The dipole interaction is defined in Figure S1.

	Monomer											
	Q											
5T	22.1											
5T-br	11.8											
5T-cho	19.9											
	Dimers											
	Q			$E_{\mu\mu}$			$E_{ele.}/E_{vdw}$			S_{ij}		
	HH	HT	TT	HH	HT	TT	HH	HT	TT	HH	HT	TT
5T-br	34.2	12.3	11.6	0.12	-0.01	0.00	3.35	13.71	12.35	-1	1	-1
5T-cho	62.3	62.0	28.0	0.30	-0.05	0.01	17.32	27.11	14.66	-1	1	-1
	Monolayers											
				$E_{\mu\mu}$			$E_{ele.}/E_{vdw}$			$\lvert S \rvert$		
5T-br				0.0200			0.59			0.73		
5T-cho				-0.1818			1.95			0.84		

Table S4 Quadrupole moments (in the unit of a.u.) of 5T monomers and dimers in different arrangements at M06-2X/6-31G* level.

	Q_{xx}	Q_{yy}	Q_{zz}	Q[a]	Q_{xy}	Q_{xz}	Q_{yz}
monomers							
5T	19.878	-1.647	-18.231	22.063	0.113	0.001	-1.420
5T-br	-5.945	11.761	-5.816	11.762	0.001	-0.001	-2.668
5T-cho	-19.583	12.733	6.850	19.875	0.012	0.029	7.233
dimers							
5T-br (HH)	-12.359	-21.438	33.797	34.201	21.959	-10.443	-20.656
5T-br (HT)	-12.314	5.673	6.641	12.327	13.224	35.286	-15.303
5T-br (TT)	10.012	-10.101	0.089	11.613	10.121	13.759	27.906
5T-cho (HH)	-46.169	-13.089	59.258	62.259	50.863	-23.419	-31.079
5T-cho (HT)	-53.558	53.820	-0.262	61.995	20.805	95.393	-8.448
5T-cho (TT)	8.312	19.025	-27.337	28.028	18.306	36.352	84.425

[a]Q is calculated as $\sqrt{\frac{2}{3}({Q_{xx}}^2 + {Q_{yy}}^2 + {Q_{zz}}^2)}$

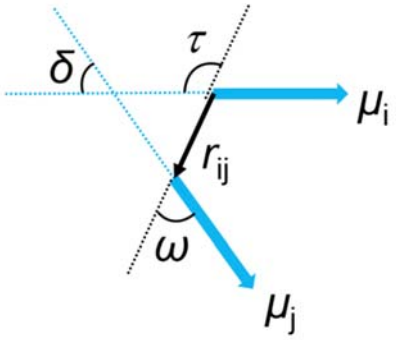

$$E_{\mu_i\mu_j} = \sum_{i<j}^{N} k_{ij} \frac{|\mu_i| \cdot |\mu_j|}{|r_{ij}|^3} (\cos\delta - 3\cos\tau \cdot \cos\omega)$$

Figure S1. Definition of dipole-dipole interaction, $E_{\mu\mu}$.

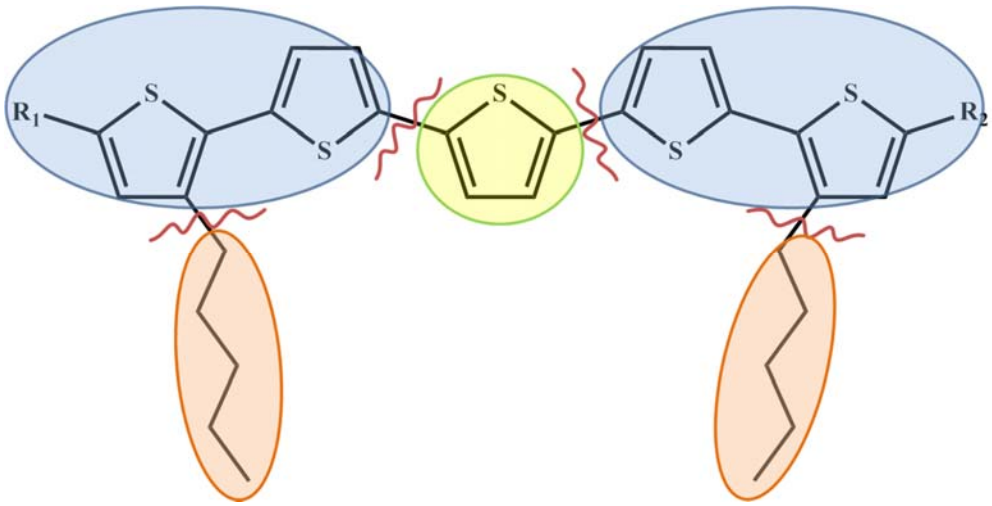

Figure S2. Fragments in the GEBF method.

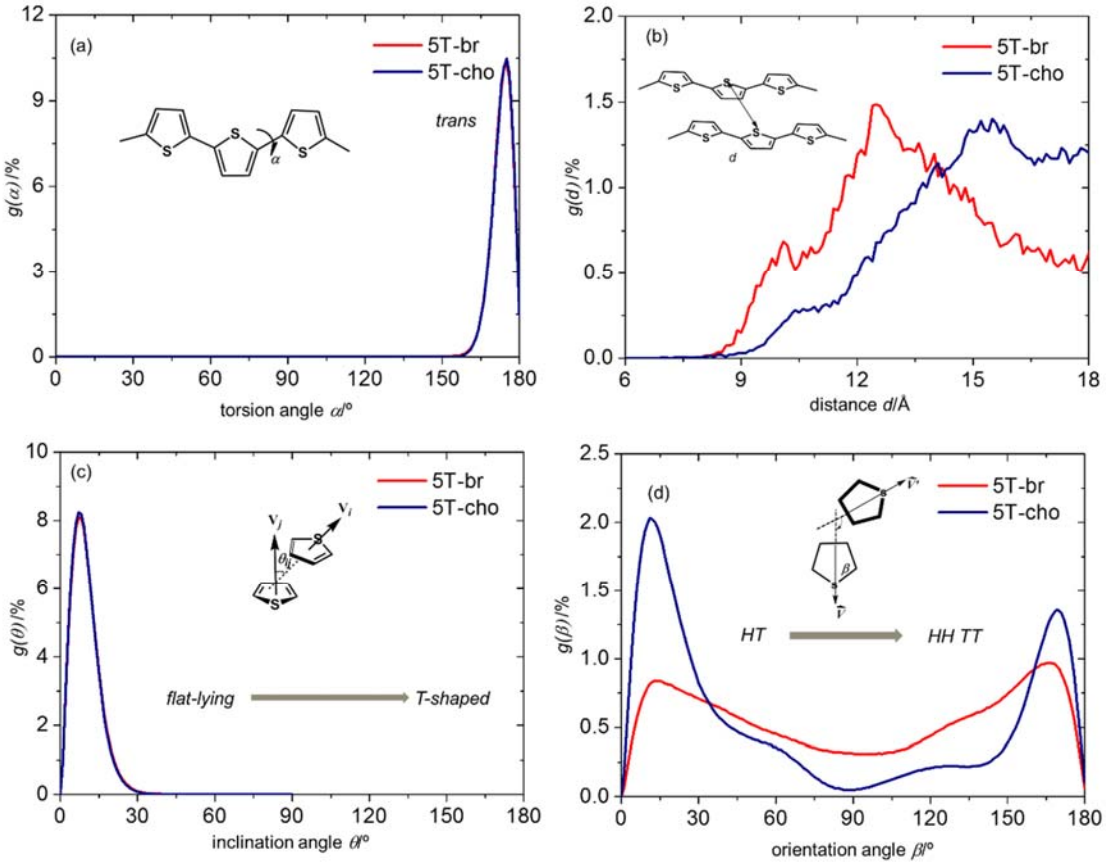

Figure S3. Statistical analysis in 5Ts monolayers on the HOPG surface, (a) torsion angle distribution, (b) radial distribution function, (c) inclination angle distribution, and (d) orientation angle distribution.

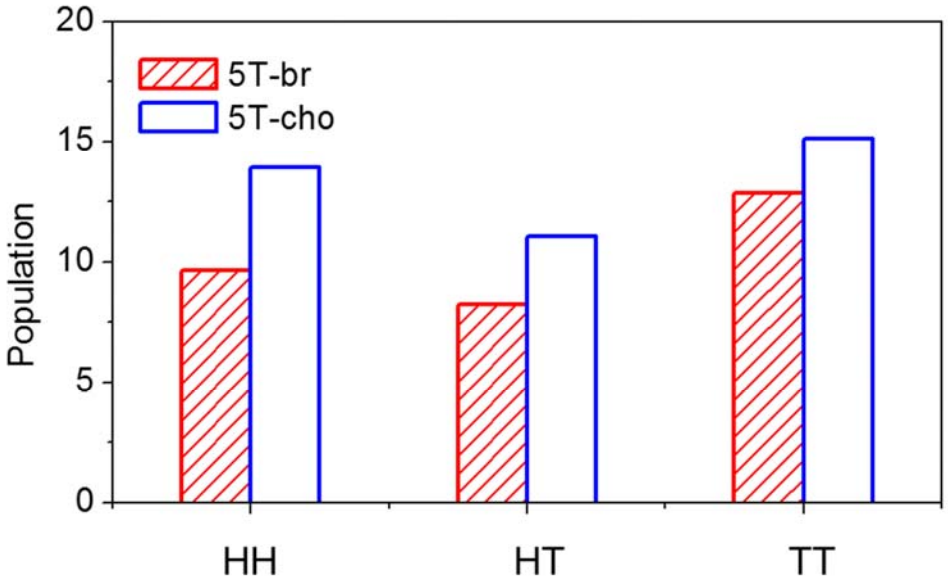

Figure S4. Distribution of HH, HT, and TT arrangements of 5T monolayers on the HOPG surface.

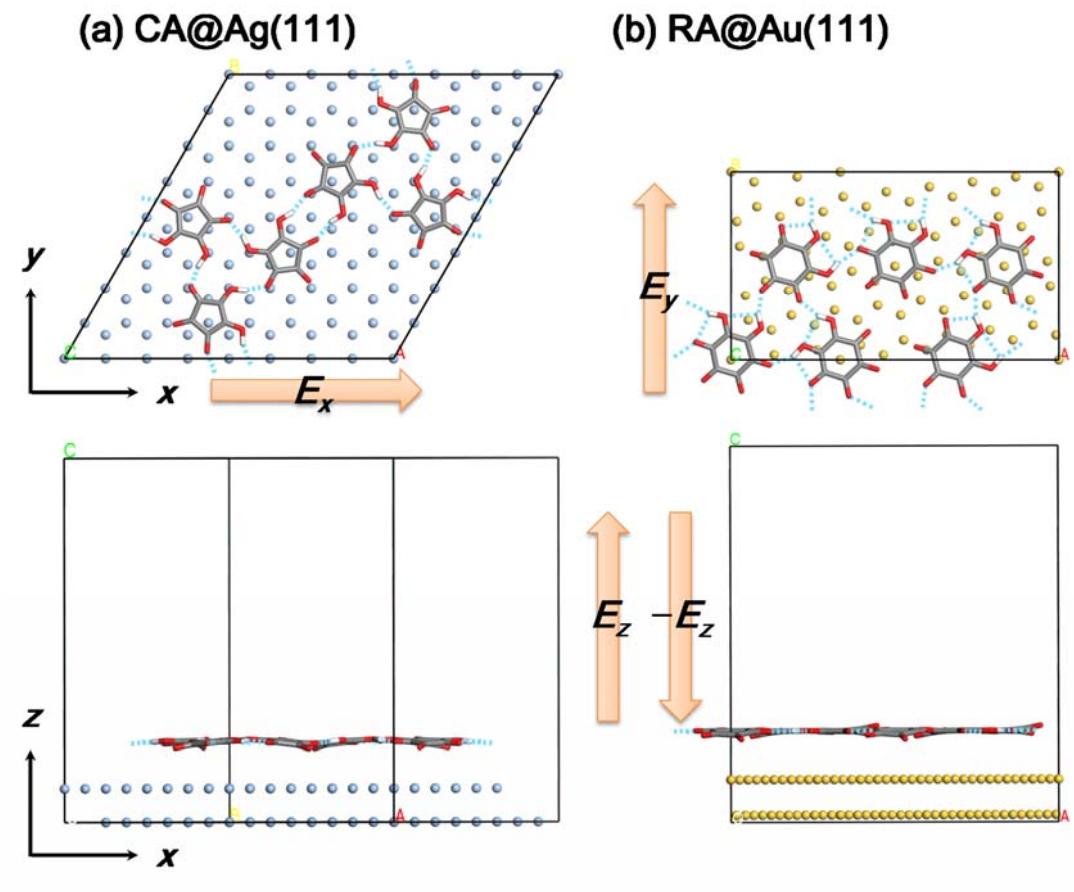

Figure S5. Initial configurations of self-assembled (a) CA monolayer on Ag(111) surface and (b) RA monolayer on Au(111) surface in our AIMD simulations. The applied electric fields for each slab model are highlighted in insets.

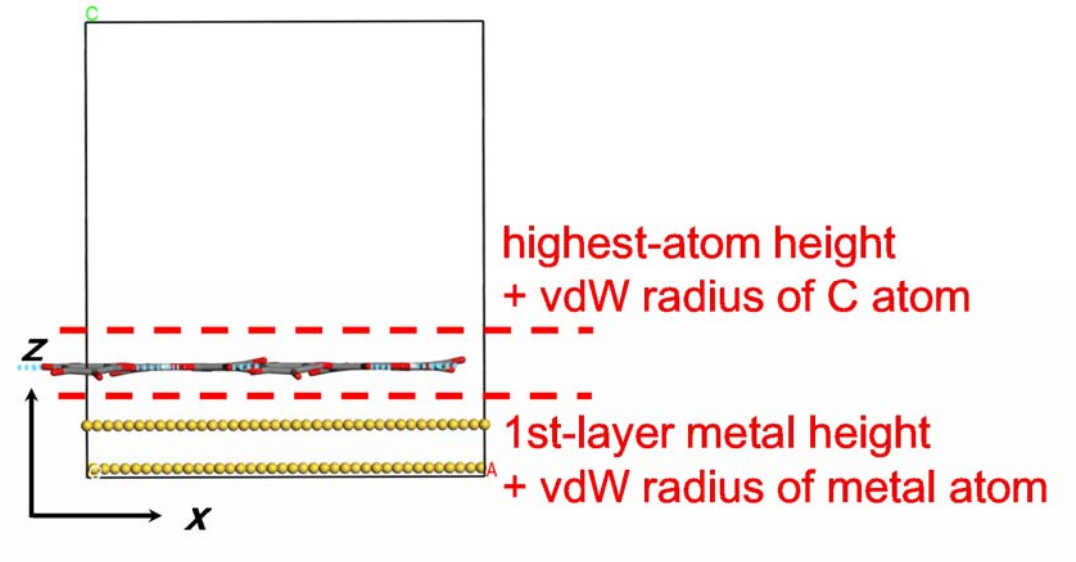

Figure S6. Illustration of two cutoffs for estimation of z component of polarization by using the charge density integral method.

References

1 K. Wang, W. Li and S. Li, *J. Chem. Theory Comput.*, 2014, **10**, 1546–1553.

2 S. Li, W. Li, T. Fang, J. Ma, W. Hua, S. Hua, and Y. Jiang, *LSQC Program*, Version 2.2, Nanjing University, Nanjing, 2012, see http://itcc.nju.edu.cn/lsqc.

3 W. Li, C. Chen, D. Zhao and S. Li, *Int. J. Quantum Chem.*, 2015, **115**, 641–646.

4 Gaussian 09, Revision **B.02**, M. J. Frisch, G. W. Trucks, H. B. Schlegel, G. E. Scuseria, M. A. Robb, J. R. Cheeseman, G. Scalmani, V. Barone, B. Mennucci, G. A. Petersson, H. Nakatsuji, M. Caricato, X. Li, H. P. Hratchian, A. F. Izmaylov, J. Bloino, G. Zheng, J. L. Sonnenberg, M. Hada, M. Ehara, K. Toyota, R. Fukuda, J. Hasegawa, M. Ishida, T. Nakajima, Y. Honda, O. Kitao, H. Nakai, T. Vreven, J. A. Montgomery, Jr., J. E. Peralta, F. Ogliaro, M. Bearpark, J. J. Heyd, E. Brothers, K. N. Kudin, V. N. Staroverov, R. Kobayashi, J. Normand, K. Raghavachari, A. Rendell, J. C. Burant, S. S. Iyengar, J. Tomasi, M. Cossi, N. Rega, J. M. Millam, M. Klene, J. E. Knox, J. B. Cross, V. Bakken, C. Adamo, J. Jaramillo, R. Gomperts, R. E. Stratmann, O. Yazyev, A. J. Austin, R. Cammi, C. Pomelli, J. W. Ochterski, R. L. Martin, K. Morokuma, V. G. Zakrzewski, G. A. Voth, P. Salvador, J. J. Dannenberg, S. Dapprich, A. D. Daniels, Ö. Farkas, J. B. Foresman, J. V. Ortiz, J. Cioslowski, and D. J. Fox, *Gaussian, Inc.*, Wallingford CT, 2009.

5 Materials studio, version 4.0. *Accelrys Inc.,* San Diego, 2006.

6 H. C. Andersen, *J. Chem. Phys.*, 1980, **72**, 2384–2393.

7 L. Verlet, *Phys. Rev.*, 1967, **159**, 98–103.

8 D. A. Kunkel, J. Hooper, S. Simpson, G. A. Rojas, S. Ducharme, T. Usher, E. Zurek and A. Enders, *Phys. Rev. B*, 2013, **87**, 41402.

9 D. A. Kunkel, J. Hooper, S. Simpson, S. Beniwal, K. L. Morrow, D. C. Smith, K. Cousins, S. Ducharme, E. Zurek and A. Enders, *J. Phys. Chem. Lett.*, 2013, **4**, 3413–3419.

10 A. Tkatchenko and M. Scheffler, *Phys. Rev. Lett.*, 2009, **102**, 073005.